Supporting Information

NIR light-triggered peroxynitrite anion production via direct lanthanide-triplet photosensitization for enhanced photodynamic therapy

*Xi Xiao,[a‡] Bingzhu Zheng,[a‡] Qiang Zheng,[b] Zijie Lu,[a] Dong Cen,[b] Xiujun Cai,[b] Xiang Li,[*a,c] and Renren Deng[*a]*

Supplementary Methods

Detection of extracellular ROS production: DPBF was used to probe the extracellular ROS generation. In a typical process, in 2 mL solution of LnNP-Ce6-PEG or LnNP@ZnO-Ce6-PEG (175 μg/mL) was added with 50 μL acetonitrile solution containing 2.5 mM of DPBF. The mixtures were irradiated with an 808 nm laser (0.5 W/cm^2 or 1 W/cm^2) for different periods (0-4 mins). The generation of ROS was measured by monitoring the absorbance changes in DPBF at 410 nm using a UV-Vis absorption spectrophotometer..

Detection of extracellular NO production: GSNO, LnNP-GSNO-PEG or LnNP@ZnO-GSNO-PEG were dispersed in PBS solution (0.16 mg/mL), followed by kept at 37 ℃ in the oven. An aliquot was taken out every 1 hour and centrifuged to obtain the supernatant for NO detection using Griess assay kits.

Detection of intracellular ROS, NO and ONOO$^-$ production: The DCFH-DA probe was used to determine ROS generation. The DAF-FM DA probe was utilized to detect NO generation. The BestBio ONOO$^-$ probe was used to detect ONOO$^-$ generation. In typical experiments, Hep 1-6 cells were incubated by 50 μg/mL of nanocomposites for three hours. After treated by NIR-light irradiation (500 mW/cm^2 at 808 nm for 2 min), a chemical fluorescent method was used to monitor the production of ROS, NO and ONOO$^-$ by adding the DCFH-DA, DAF-FM DA and BestBio ONOO$^-$ probes, respectively. The cells were incubated for another 20 min before they were observed by a fluorescence microscope.

Biosafety assessment: To verify the biosafety of the materials, the major organs (heart, liver, spleen, lung, and kidney) in each group were collected on Day 14. The samples were formalin-fixed and paraffin-embedded for permanent staining by hematoxylin and eosin. The blood samples at Day 1, Day 3 and Day 7 were also collected for blood biochemistry assay and blood routine examination at clinical laboratory of Sir Run Run Shaw Hospital.

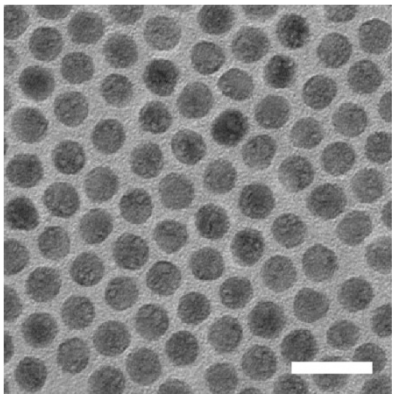

Fig S1. Transmission electron microscopy (TEM) images of the as-synthesized LnNP nanoparticles. The scale bar is 20 nm.

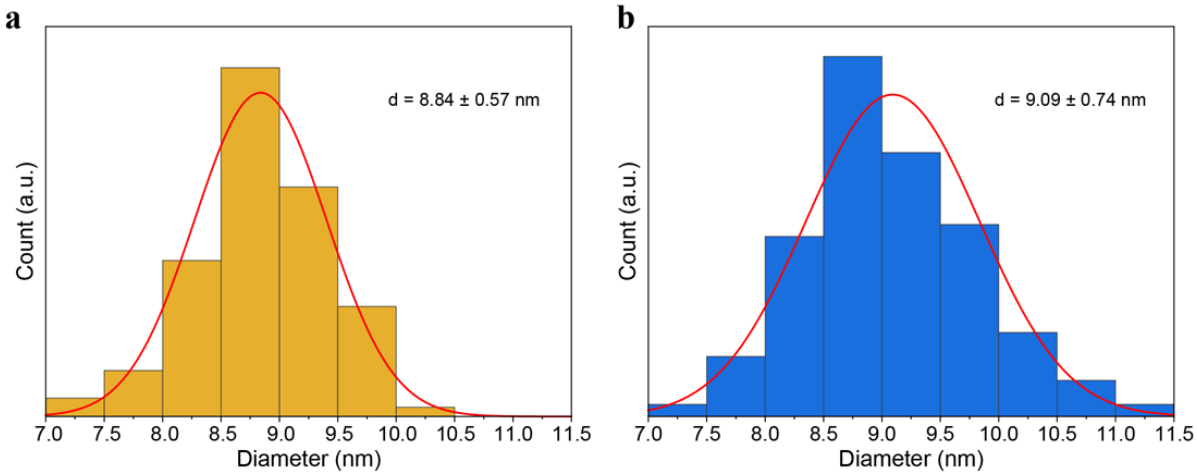

Fig S2. (**a**) Size distribution of LnNP nanoparticles. (**b**) Size distribution of LnNP@ZnO nanoparticles.

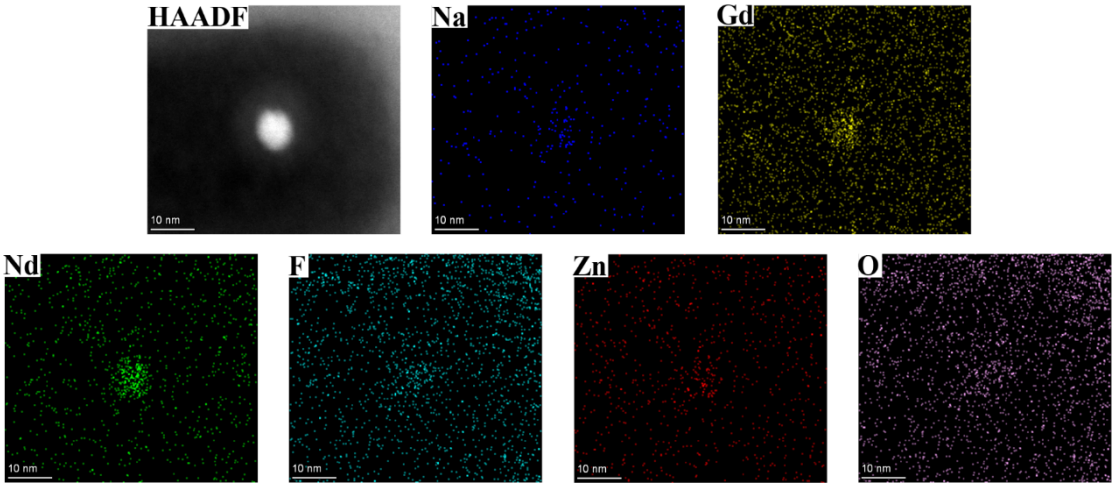

Fig S3. Element mapping images of a typical LnNP@ZnO particle.

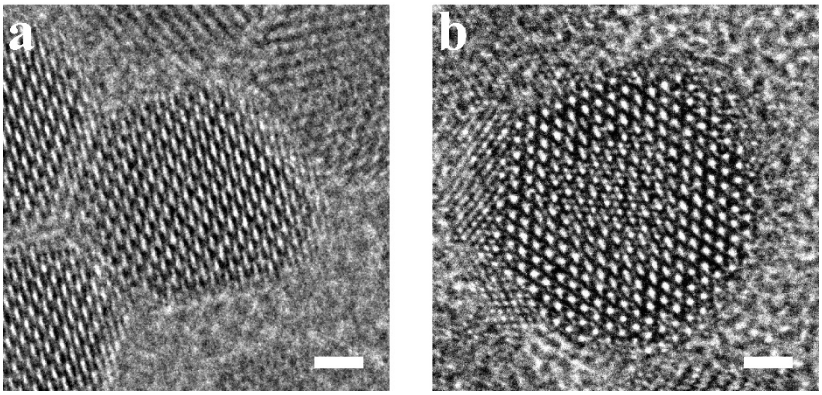

Fig S4. High-resolution TEM (HRTEM) images of the as-synthesized (**a**) LnNP nanoparticles and (**b**) LnNP@ZnO nanoparticles. The scale bar is 2 nm.

a

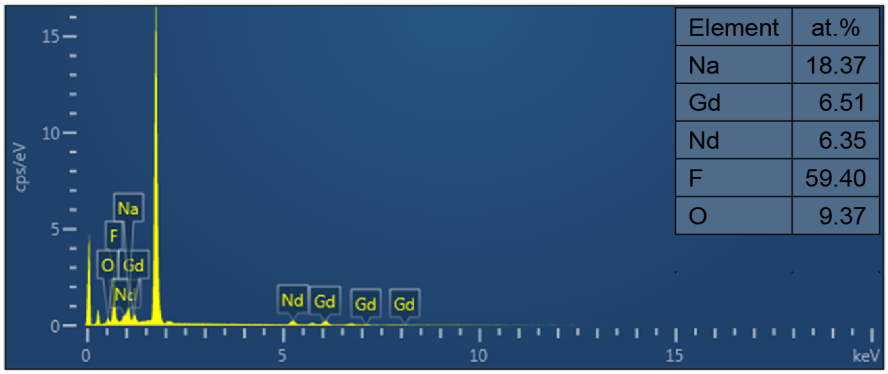

b

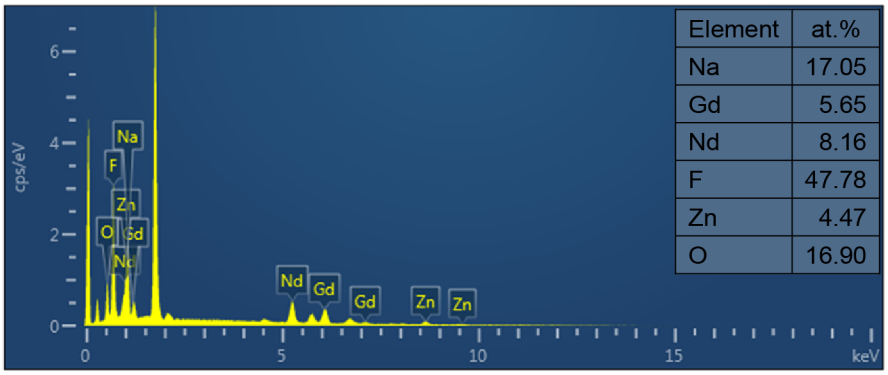

Fig S5. Energy dispersive spectroscopy (EDS) of (**a**) LnNP and (**b**) LnNP@ZnO powder on silicon wafer.

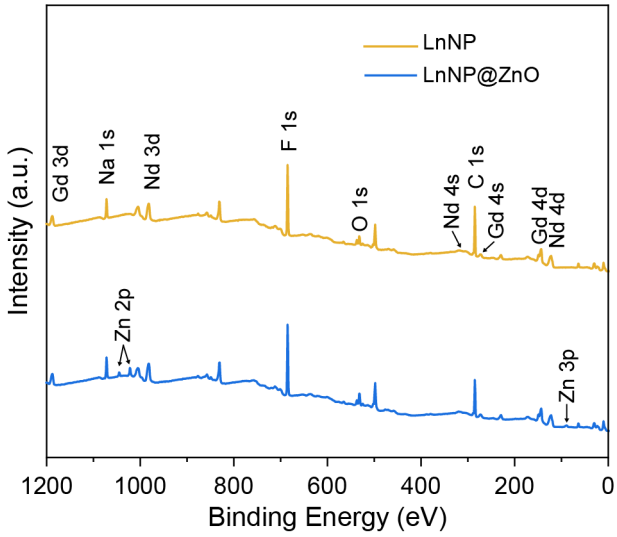

Fig S6. X-ray photoelectron spectroscopy (XPS) spectrum of LnNP and LnNP@ZnO powder.

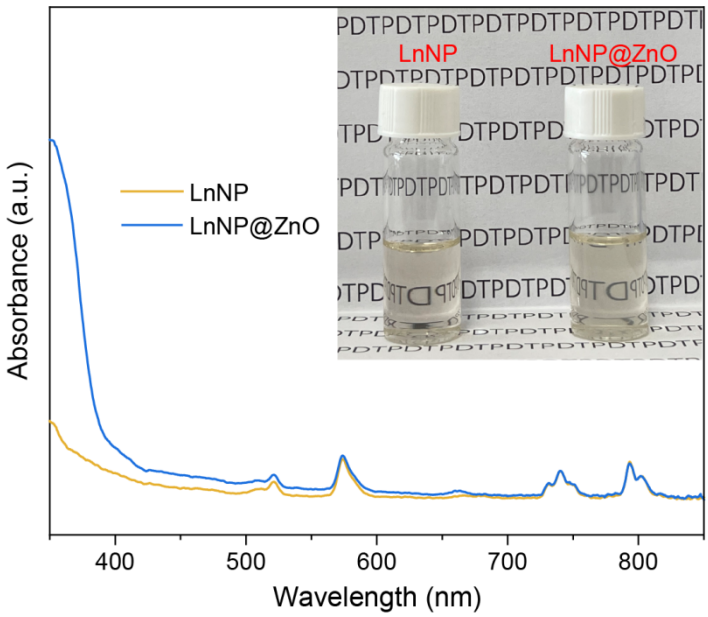

Fig S7. UV-vis absorption spectra of LnNP and LnNP@ZnO in cyclohexane. Inset: photo of corresponding solution.

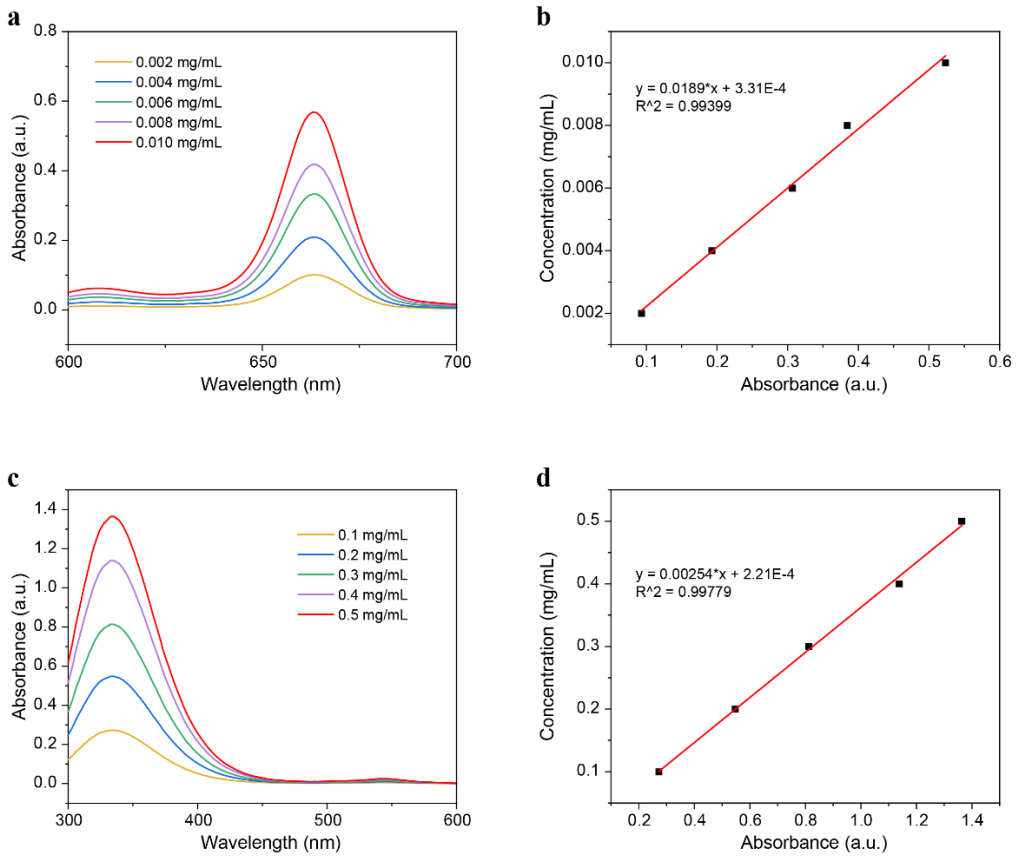

Fig S8. (**a-b**) UV-Vis spectra of Ce6 solutions at different concentrations and the plot of the Ce6 calibration dataset showing the change in absorbance of Ce6 at 660 nm as a function of concentration. (**c-d**) UV-Vis spectra of GSNO solutions at different concentrations and the plot of the GSNO calibration dataset showing the change in absorbance of GSNO at 334 nm as a function of concentration.

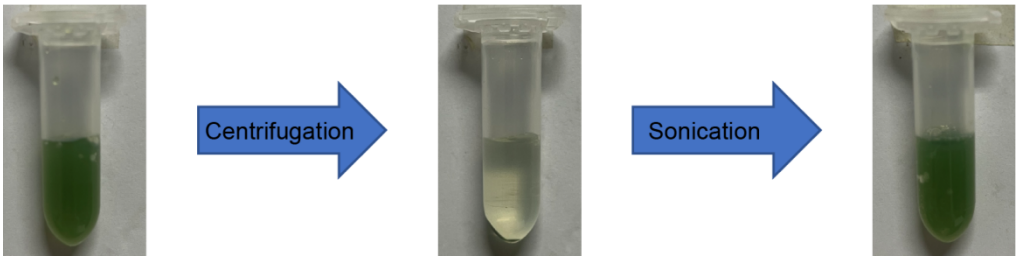

Fig S9. Photos of LnNP@ZnO-Ce6/GSNO-PEG nanocomposites in deionized water before and after centrifugation.

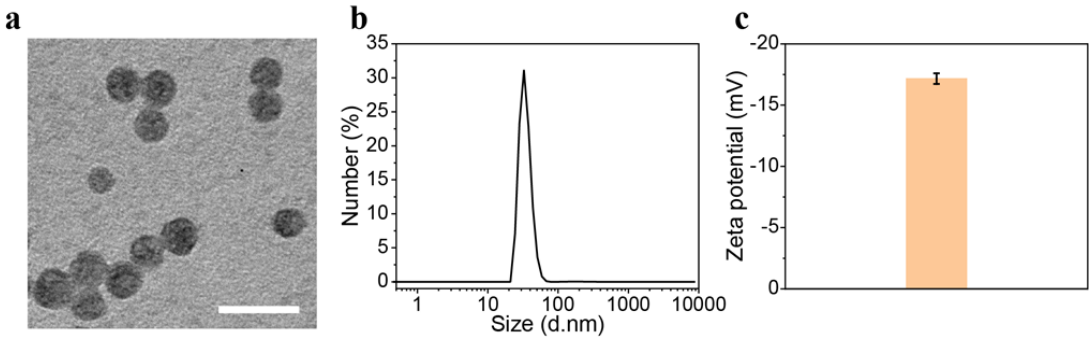

Fig S10. (**a**) TEM image of LnNP@ZnO-Ce6/GSNO-PEG. The scale bar is 20 nm. (**b**) Dynamic Light Scattering (DLS) measurements showing the size distribution of LnNP@ZnO-Ce6/GSNO-PEG. (**c**) Zeta potential of LnNP@ZnO-Ce6/GSNO-PEG.

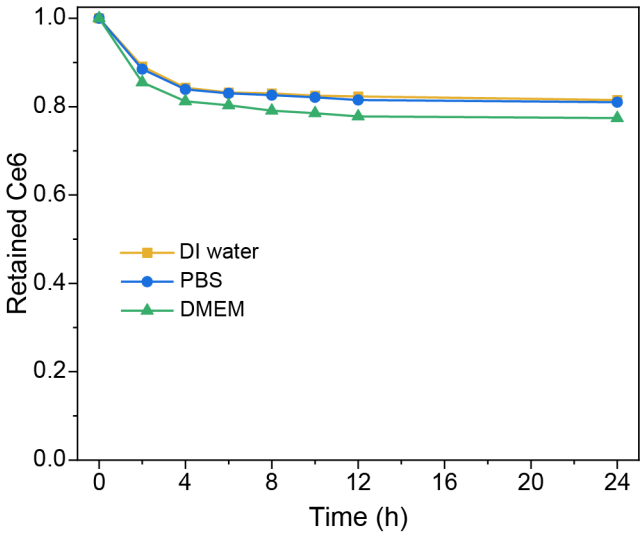

Fig S11. Time-dependent Ce6 release curves of LnNP@ZnO-Ce6/GSNO-PEG dispersed in DI water, PBS and Dulbecco's modified eagle medium (DMEM, containing 10% Newborn Calf Serum).

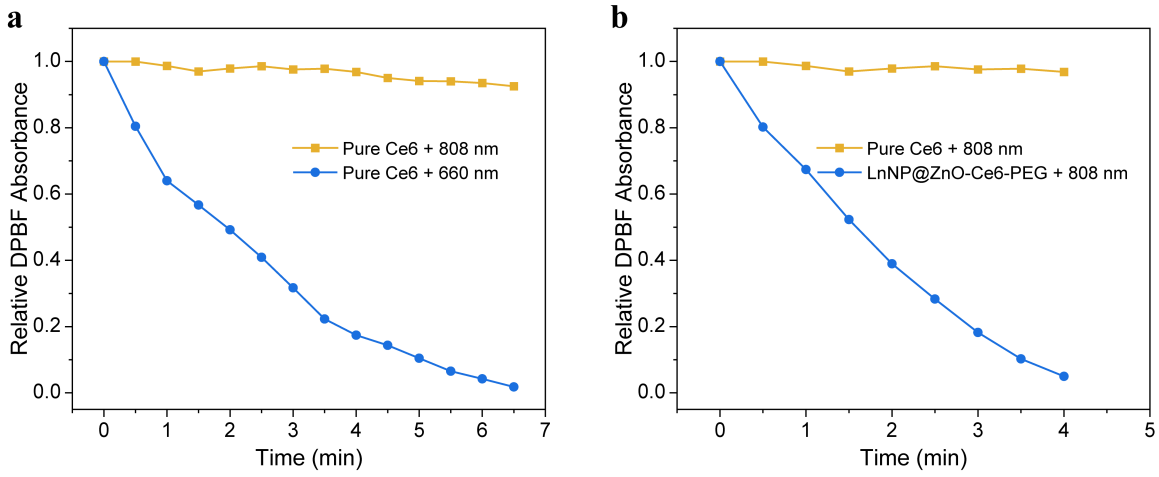

Fig S12. Plot of relative absorbance change of 1,3-diphenylisobenzofuran (DPBF) as a function of time, indicating the ROS generation rate of (**a**) pure Ce6 molecules under 808 nm/660 nm irradiation and (**b**) pure Ce6 molecules and LnNP@ZnO-Ce6-PEG nanocomposites under 808 nm irradiation.

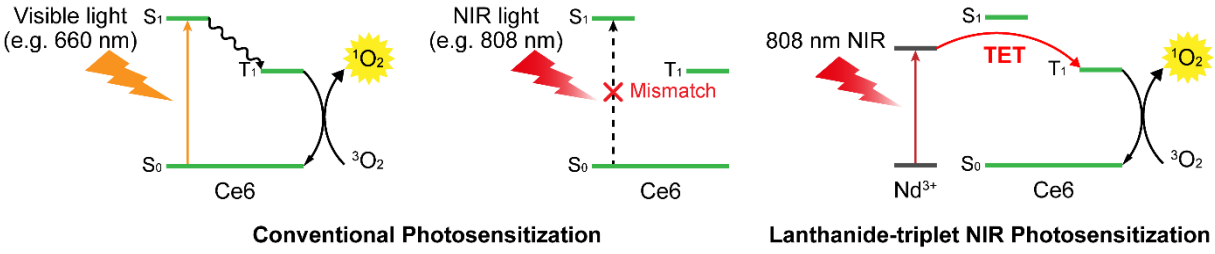

Fig S13. Schematic comparison of conventional photosensitization of Ce6 and direct lanthanide-triplet NIR photosensitization of Nd^{3+}-Ce6 to generate singlet oxygen.

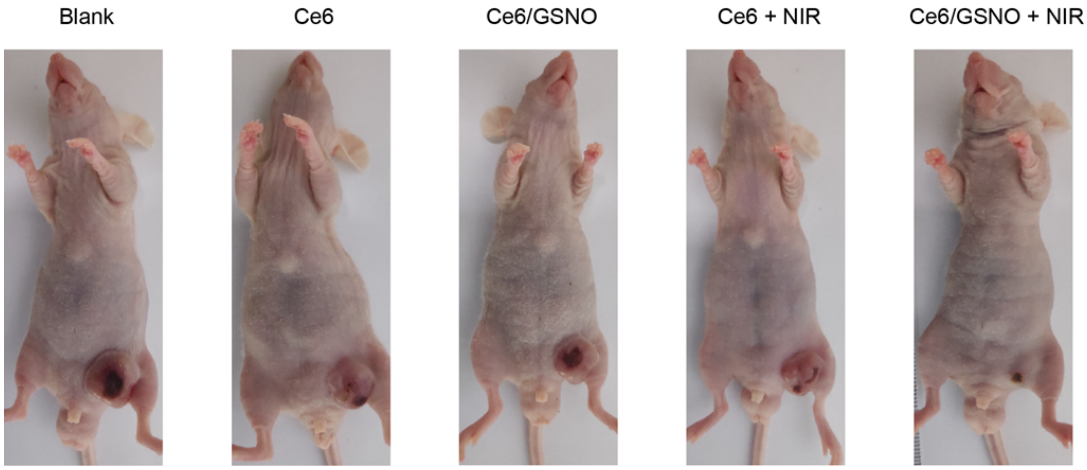

Fig S14. Photographs of treated mice at D14 after different treatments.

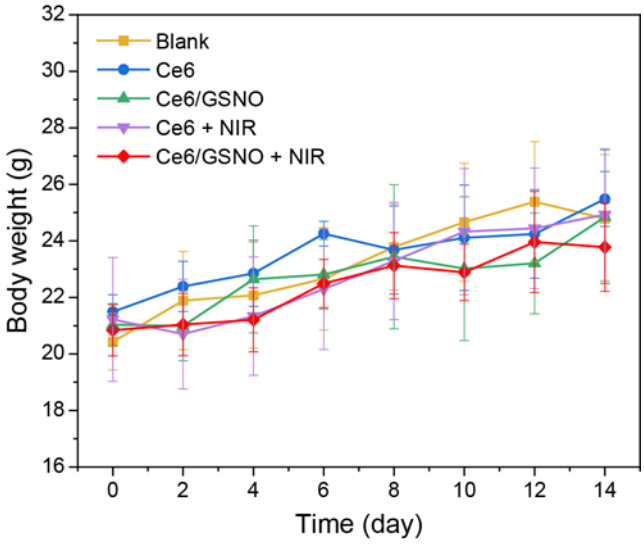

Fig S15. Changes in body weight of mice with Hep 1-6 liver tumor after different treatments. The error bars represent standard deviation for n = 5.

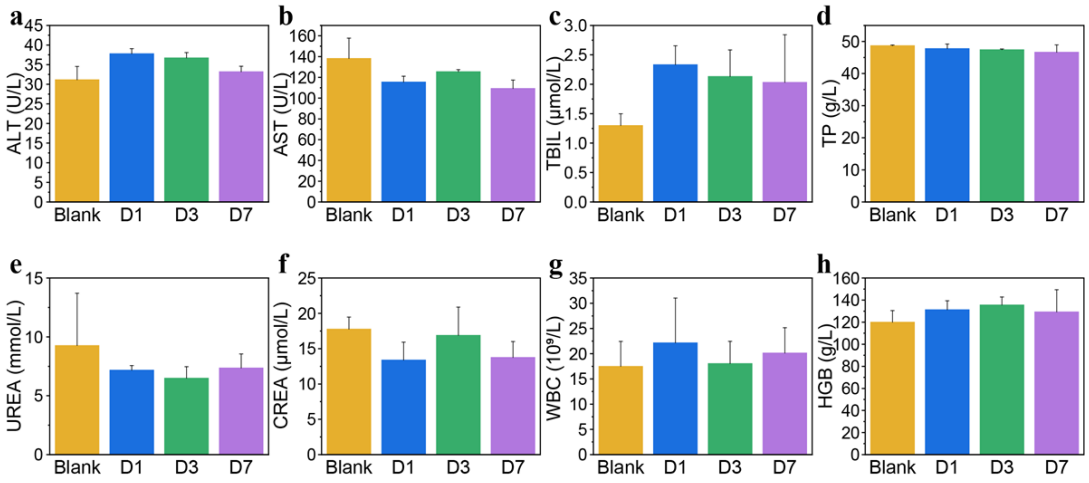

Fig S16. (**a-h**) Blood biochemistry and hematological analysis of mice after intratumorally injection of LnNP@ZnO-Ce6/GSNO-PEG, including alanine aminotransferase (ALT), aspartate aminotransferase (AST), total bilirubin (TBIL), total protein (TP), urea, creatinine (CREA), white blood cell (WBC) and hemoglobin (HGB) recorded on day 1, day 3 and day 7. The error bars represent standard deviation for n = 3.

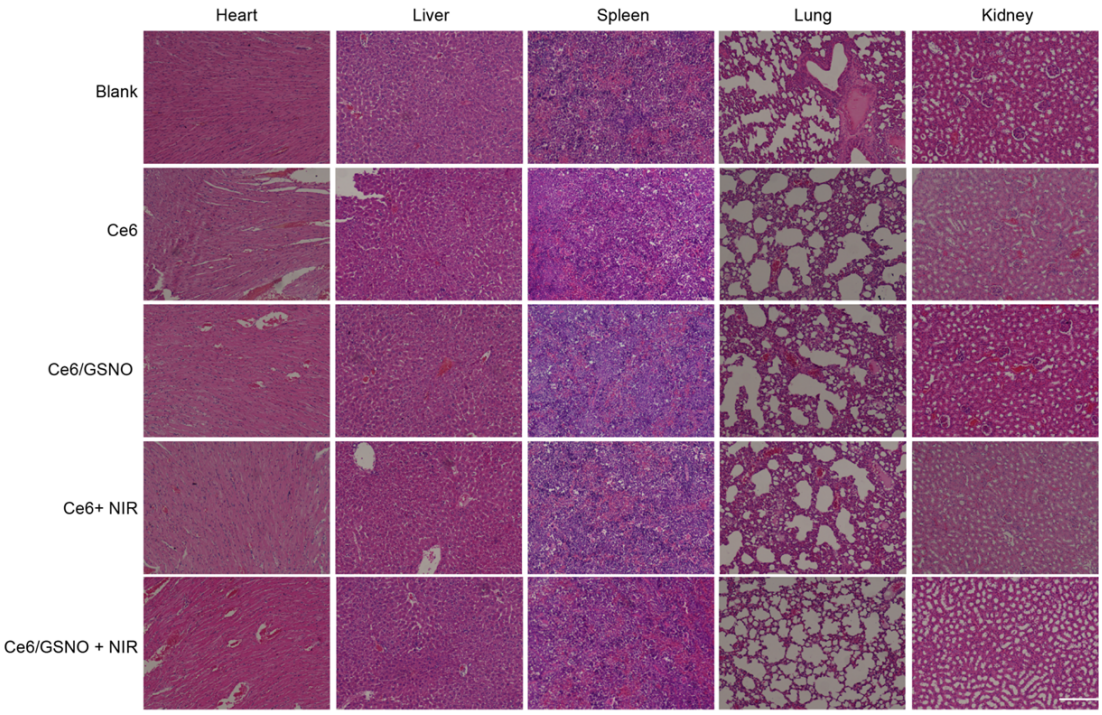

Fig S17. H&E staining of the major organs (heart, liver, spleen, lung and kidney) of mice to examine the pathologica changes after different treatments in 14 days. The scale bar is 200 μm.

Table S1 Elemental composition of LnNP and LnNP@ZnO obtained from inductively coupled plasma mass spectrometry (ICP-MS) analysis.

	Gd	Nd	Zn
LnNP	1.00	1.27	/
LnNP@ZnO	1.00	1.34	0.62